Vietnam Journal of Science and Technology ***63*** *(2) (2025) 285-296*

doi:10.15625/2525-2518/18203

Fabrication and characterization of pulsed electron beam deposited TiO_2 thin films with glancing angle deposition techniques for biosensing application

Quang-Duy Dao[1, *] Tri-Nghia Nguyen[1], Duy Thien Nguyen[1], Tung Nguyen Dinh Hai[1], Thi Huong Vu[2], Tuan Tu Le[1], Thanh Mai Vu[3, 4], Van Vu Le[1]

[1]*Faculty of Physics, University of Science, Vietnam National University, Hanoi, 334 Nguyen Trai, Thanh Xuan, Ha Noi, Viet Nam*

[2]*Falculty of Chemistry, Hanoi National University of Education, 136 Xuan Thuy, Cau Giay, Ha Noi, Viet Nam*

[3]*Research Institute of Sciences and Engineering, University of Sharjah, PO.BOX, 27272, Sharjah, United Arab Emirates*

[4]*Department of Mechanical and Nuclear Engineering, University of Sharjah, PO.BOX, 27272, Sharjah, United Arab Emirates*

[*]Emails: *daoquangduy@hus.edu.vn*

Received: 30 March 2023; Accepted for publication: 19 July 2023

Abstract. We demonstrated fabrication and characterization of TiO_2 thin films using pulsed electron deposition (PED) with glancing angle deposition (GLAD) techniques. The X-ray diffraction patterns and Raman spectra indicated that the fabricated TiO_2 thin films were formed in anatase phases with crystallite sizes of around 20.3 nm. By using the GLAD techniques, the surface morphology and optical properties of TiO_2 thin films were well controlled. In particular, the rod-like nanoparticles were probably raised up and the smoothness of the thin films was reduced when incident angles increased from 0º to 70º, which resulted from the self-shadowing mechanism. The absorption coefficient was reduced, the energy band gap increased, and the Raman peaks at 144 cm^{-1} were vanished with increasing in incident angles in part due to changes in the thin film porosity and the crystallite sizes, which is proportional to the number of self-shadowed induced voiding sites. Furthermore, the non-enzymatic fluorescent glucose sensor using the PED-based TiO_2 thin films was demonstrated to explore the application potential of the fabricated materials.

Keywords: thin film, glancing angle deposition, titanium dioxide, pulsed electron deposition.

Classification numbers: 2.4.2, 2.5.2.

1. INTRODUCTION

Recently, titania (TiO_2) thin films are attracting enormous research interest from the scientific community because of their potential application in various fields, such as photocatalysis, lithium-ion battery, and electron transport materials in photovoltaic devices [1 -

6]. In nature, rutile, anatase, and brookite are main crystalline structures of TiO_2 materials. While the rutile phase is most stable, the anatase phase exhibited higher potential application than the others in part due to their energy band gap, surface orientation, and charge transport [7 - 9]. TiO_2 thin films are the most widely utilized photocatalyst for decomposition of organic pollutants [10 - 12]. Although the photocatalytic activity of TiO_2 thin films still remains incompletely illustrated, it is well recognized that the photocatalytic reaction is triggered by the band gap excitation of TiO_2 material, followed by the formation of electrons in conduction band and holes in valence band [2]. Those electron-hole pairs then caused generation of reactive species, such as $^{*}OH$, H^{+} and $^{*}O_2^{-}$, which directly insult in the oxidation processes leading to the degradation of organic pollutants [2, 13]. Therefore, the efficiency of TiO_2 photocatalyst systems strongly depends on the surface morphology of nanostructure films, in which organic pollutants are adsorbed. Moreover, there have been various researches done on TiO_2-based sensors for glucose detection, in which TiO_2 material acts as a direct photocatalyst in non-enzymatic glucose sensors owing to its enhanced surface to volume ratio [14, 15]. On the other hand, TiO_2 thin films were also employed widely in perovskite solar cells as an electron transport layer [4, 16]. The TiO_2 electron transport layer does not only play the key roles as a scaffold to extend the interface areas of perovskite absorber and reinforce the crystallization of perovskite crystals, but also to prevent the formation of unexpected PbI_2 crystals, based on controlling the surface morphology of the TiO_2 thin films [17 - 19]. It means that controlling the surface morphology of thin film and/or the shape of nanoparticles in thin film is essential to extending and improving the potential application of the TiO_2 thin films.

Few methods were demonstrated successfully for the fabrication of TiO_2 thin films, namely wet chemical synthesis, pulsed laser deposition (PLD), and sputtering deposition [20 - 23]. Compared to wet chemical methods, PLD as well as other physical methods produced the TiO_2 thin films with higher purity and reproducibility. The research on the TiO_2 thin film deposited using PLD was extensively conducted and this technique was considered as a potential technique because of several following reasons: (*i*) the stoichiometric compositions of the films fabricated were identical to that the target materials made of, (*ii*) the deposition rate was high, and (*iii*) the film growth was easily controlled using deposition parameters, such as substrate temperature, chamber pressure, and source energy [22, 24 - 26]. For TiO_2 thin film fabrication, there existed another physical method similar to PLD, namely pulsed electron deposition (PED). The PED, which utilized a pulsed high power electron beam instead of laser beam to transport materials from a target to substrates, shared the wonderful advantages with PLD. Furthermore, by using charged electrons, PED technique could handle ultra-violet-transparent materials. However, the fabrication of TiO_2 thin film using PED was hardly carried out in part owing to emerging large particles with the sizes of micrometer on the deposited films. Furthermore, the PED based TiO_2 thin films were relatively dense and compact, which limited their applicability in sensor technology. On the other hand, physical methods, such as PLD and sputtering deposition are often gone along with glancing angle deposition (GLAD) technique to easily control the shape of nanoparticles and/or the surface morphology of the thin films [27]. During the GLAD progress, the vapor flux is deposited onto the substrates at a large angle with respect to the substrate normal, forming various nanostructures, such as nanorods and nanopillars [28, 29]. Herein, we demonstrated fabrication of TiO_2 thin films by using PED cooperating with GLAD techniques. The prepared TiO_2 thin films were investigated using various analytical techniques and the effects of GLAD technique on the crystallite structure, surface morphology and optical and electronic properties were taken into account. Furthermore, the non-enzymatic glucose sensor using the PED-based TiO_2 thin films was demonstrated.

2. MATERIALS AND METHODS

TiO_2 thin films in this study were deposited on glass substrates inside pulsed electron evaporator incorporating GLAD technique, as shown in Figure 1. The glass substrates were cut into 0.8 × 0.8 cm^2 and subsequently cleaned with detergent, water, acetone, and isopropyl alcohol. After drying processes at 70 ºC for 30 minutes, the glass substrates were transferred to a pulsed electron evaporator chamber, in which the pressure remained at 7.5×10^{-4} Pa for 2 hours. Electron beams were generated with applied bias of 14 kV, which produces the single pulsed energy of around 0.35 J. The distance from the tube end to target was around 0.5 cm. The beam radius and pulsed energy density were 0.2 cm and 2.8 J/cm^2, respectively. During deposition processes, the oxygen gas was introduced at the rate of 19.2 sccm and the chamber pressure was kept at 6.8×10^{-1} Pa. The number of electron pulses was 30000. As a result, the synthesized TiO_2 thin films have a thickness of around 50 nm. In this study, the GLAD techniques were applied with the incident angles of 0º, 20º, 45º, 60º, and 70º. All as-deposited samples were thermally annealed in air for one hour at 500 or 600 ºC. The TiO_2 target with radius of 4.8 cm was prepared by mixing 7.34 gram of TiO_2 nanoparticles (Sigma-Aldrich) and 0.15 gram of polyvinyl alcohol (PVA, Himedia). We note that the TiO_2 nanoparticles used for the fabricated targets have relatively small average sizes of 21 nm. The products were then pressed under 5 tons to get the desired shapes. Before using, the TiO_2 targets were annealed at 1100 ºC for 6 hours to recrystallize the TiO_2 nanoparticles as well remove PVA and remaining organic compounds.

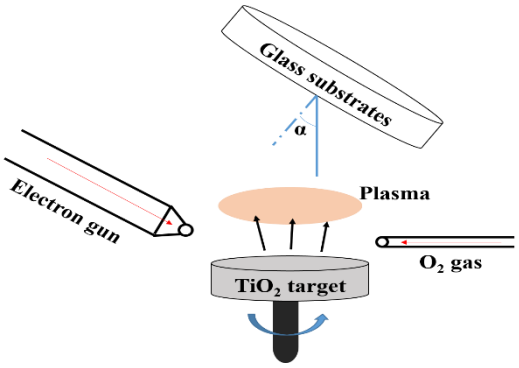

Figure 1. A schematic diagram of pulsed electron deposition with glancing angle technique.

The absorbance spectra of the TiO_2 thin films in this study were estimated using a spectrophotometer (UV-2450, Shimadzu). The surface morphology of the TiO_2 thin films with the various incident angles were observed using field-emission scanning electron microscopy (FESEM, S-4800 Hitachi) with the operating voltages of 5.0 kV. The Raman spectra of the TiO_2 thin films were estimated using a Raman spectrometer (Labram 800, Horiba) using the excitation lasers with the wavelengths of 632.8 nm. The X-ray diffraction (XRD) patterns of the TiO_2 thin films were measured by an X-ray diffractometer (Empyrean, Malvern Panalytical) using Cu Kα radiation with the wavelength (λ) of 0.15406 nm. The photoluminescence (PL) spectra of the fabricated TiO_2 thin films were measured using a fluorescence spectrophotometer (Fluorolog, Horiba). For simple glucose sensing measurements, β-D glucose, hereafter referred to as glucose, were dissolved into deionized water to produce the glucose solutions with the different concentrations, which then poured into 3 mL quartz cuvettes. In particular, 0.2972 gram of glucose were dissolved into 3 mL of deionized water to produce the precursor solution

(0.5 M) and the measured glucose solutions were generated by diluting the precursor solution with deionized water. The TiO_2 thin films with the 0º-incident angles were immersed into the glucose-filled-up quartz cuvette for the PL measurements. We note that the TiO_2 thin films were excited with 315-nm wavelength photons.

3. RESULTS AND DISCUSSION

The crystallite structure of the TiO_2 thin films in this study were analyzed using an X-ray diffractometer.

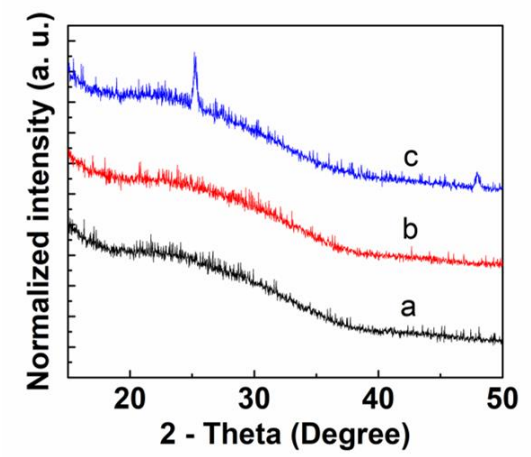

Figure 2. XRD patterns of TiO_2 thin films: (a) without thermal annealing, and with thermal annealing at (b) 500 ºC and (c) 600 ºC.

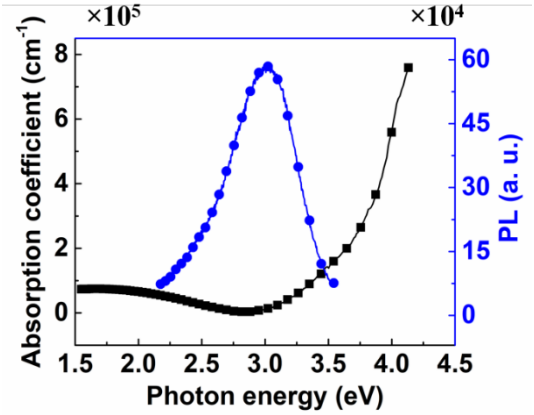

Figure 3. Absorption (filled rectangles) and PL (filled circles) spectra of TiO_2 thin films.

Figure 2 exhibits the XRD patterns of the as-deposited TiO_2 thin film and the TiO_2 thin films with thermal annealing at the different temperatures. There were no peaks observed in the XRD patterns of the as-deposited TiO_2 thin films or the TiO_2 thin film which thermal annealed at the low temperatures of 500 ºC for 1 hour. The absence of the diffraction from TiO_2 thin films could result from the disorder of the TiO_2 nanoparticles in the fabricated thin film and/or the finite resolution of the x-ray diffractometer. However, the TiO_2 nanoparticles in amorphous phases were recrystallized when the TiO_2 thin films were thermal annealed at the temperature of 600 ºC for 1 hour. The TiO_2 thin films with the thermal annealing at 600 ºC exhibited the XRD

patterns with the relatively strong diffraction peaks at 25.3° and 47.9°, corresponding to the (101) and (200) crystal planes of the TiO_2 anatase phase (JCPDS-ICDD card: 21-1272), respectively [30, 31]. Furthermore, the XRD patterns of the 600 ºC annealed TiO_2 thin films were compatible with those of the TiO_2 anatase phase. Although more research is required to confirm the crystal structure of the fabricated thin films, we suggested that the TiO_2 thin films in this study were the anatase phase. Using the Debye-Scherrer relation, the crystallite size of the TiO_2 nanoparticles in the fabricated thin films were estimated to be around 20.3 nm. The lattice parameters of the fabricated TiO_2 thin films were calculated. It indicated that the lattice parameters for anatase phase (tetragonal structure) of the TiO_2 thin films in this study were a = b = 3.791 Å and c = 9.598 Å. As a result, the cell volume of 137.91 $Å^3$ was achieved. The calculated lattice parameters of the fabricated TiO_2 thin film are in good agreement with the standard JCPDS pattern of anatase (21-1272). On the other hand, we did not observe any peak related to the TiO_2 rutile phase in the XRD patterns even though the TiO_2 thin films were thermal annealed at 600 ºC for 1 hour. We suggest that the relatively high temperatures of amorphous-anatase phase transitions probably originated from the small size of the TiO_2 nanoparticles in the thin films deposited from the targets with the small-size TiO_2 nanoparticles [7].

Furthermore, the optical properties of the TiO_2 thin films in this study were also investigated. Figure 3 shows the absorption coefficient and PL spectra of the TiO_2 thin film with thermal annealing at 600 ºC for 1 hour. The indirect band gap energy of the fabricated TiO_2 thin films, which was estimated from a plot of $(\alpha hv)^{1/2}$ vs. photon energy (hv), was around 3.45 eV. The band gap energies of bulk TiO_2 materials, which are mainly ascribed to the gap between the energy levels of O 2p (valence band) and Ti 3d (conduction band) orbitals, are well known to be 3.2 eV [32]. The relatively high band gap energies implied the sizes of TiO_2 nanoparticles in the fabricated thin films is small ($\leq$ 25 nm), which is in good agreement with the aforementioned amorphous-anatase phase transition temperatures [33, 34]. Otherwise, the TiO_2 thin film exhibited the PL spectra with a strong peak at around 413 nm (corresponding to 3 eV). The strong PL peak at around 413 nm possibly resulted from band edge free excitons. Those emission is attributed to indirect transition X_{1a} and Γ_{1b} and linked to exciton recombination in shallow trapped surface states [30, 35].

To obtain nanoparticle shape and surface morphology, the fabricated TiO_2 thin films were investigated by scanning electron microscopy. Figure 4 shows the top-view SEM images of the TiO_2 thin films with the different incident angles. The TiO_2 thin film (Figure 4a and Figure 4e) with the incident angles of 0º, in which the TiO_2-vapor trajectories were perpendicular to the glass substrates, exhibited the relatively smooth surface with the few large particles. The large particles on the thin film surfaces were in part attributed to the high energy densities of the incident electron beams. However, by increasing the incident angles, the surface morphology of the TiO_2 thin films were drastically changed with decreasing in the smoothness. Although more efforts should be required to confirm clearly the particle shapes, the rod-like particles seem to have appeared on the surface of the TiO_2 thin films fabricated as the incident angles were higher than 60º. We suggest that the self-shadowing phenomena occurred when the incident angle increased to 60º or 70º, which leads to voiding within the relatively high incident-angle deposited TiO_2 thin films [29, 36, 37]. In those voiding or shadowed surfaces, TiO_2 nanoparticles were deposited by some mechanisms other than direct impingement, for example, by surface diffusion of adatoms from non-shadowed surfaces and/or by indirect impingement of vapor atoms which have been previously desorbed, reflected, or scattered [29]. As a result, the smoothness was reduced and the rod-like nanoparticles were raised up. Controlling successfully

the morphology of the TiO_2 thin films using the GLAD techniques will enlarge the potential of TiO_2 materials in photovoltaic devices and sensor applications [27, 31].

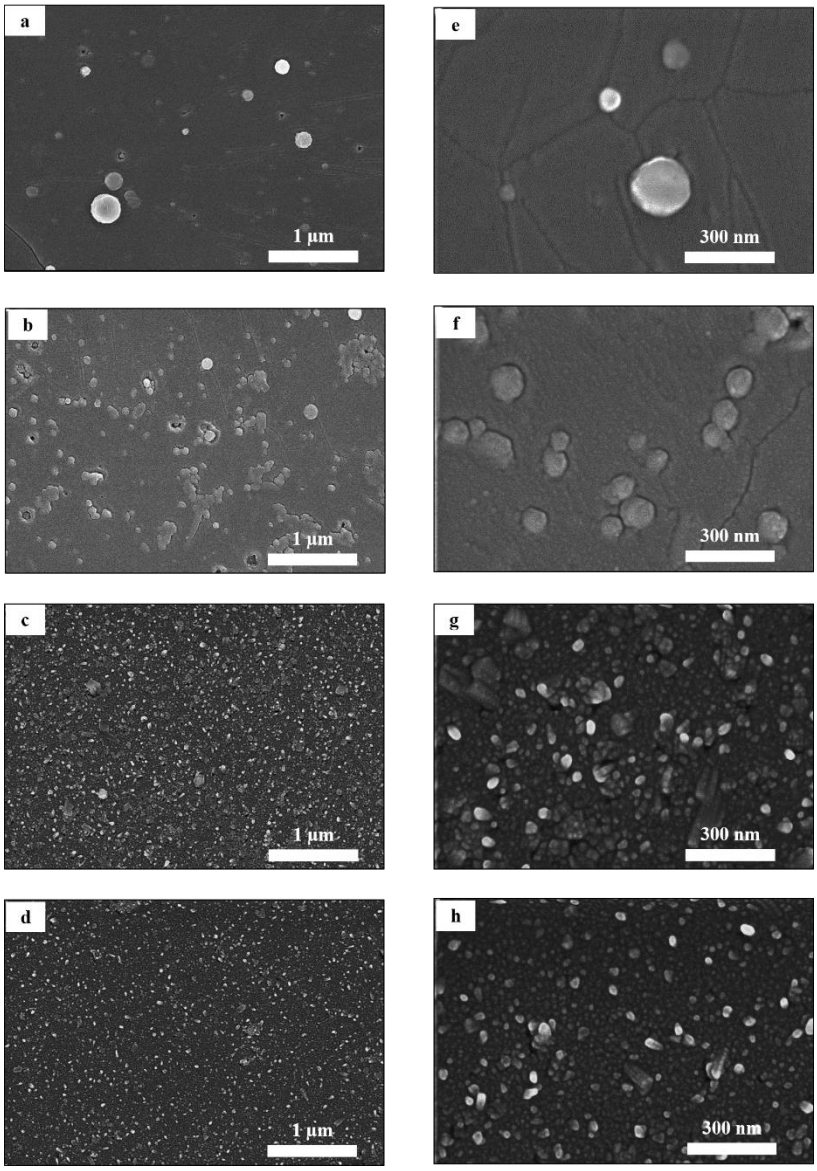

Figure 4. SEM images of TiO_2 thin films with incident angles of: (a) and (e) 0º, (b) and (f) 20º, (c) and (g) 60º, and (d) and (h) 70º.

Figure 5(a) shows Raman spectra of the fabricated TiO_2 thin films with the different incident angles. We note that all the TiO_2 thin films were thermally annealed at 600 ºC for 1 hour. The Raman spectra of the TiO_2 thin films with the 0º-incident angles exhibited the relatively strong peaks at 144 cm^{-1} corresponding to the anatase phases [6, 38]. Although more research is required to confirm the crystal structure of the fabricated thin films, those results implied that TiO_2 thin films in this study were the anatase phase. However, the full width at half maximum of the Raman peaks at 144 cm^{-1} were slightly enlarged when the incident angles

increased to 20º, and those Raman peaks vanished when the incident angles increased to 60º or 70º. Furthermore, there were no signals of diffraction peaks at 25.3°, corresponding to the (101) crystal planes of the TiO_2 anatase phase, observed in the XRD patterns of the fabricated TiO_2 thin films as the incident angles were higher than 60º, as shown in Figure 5(b). We suggest that disappearing the Raman peaks at 144 cm^{-1} and the diffraction peaks at 25.3° probably resulted from increasing in the thin film porosity, which is proportional to the number of self-shadowed induced voiding sites [39].

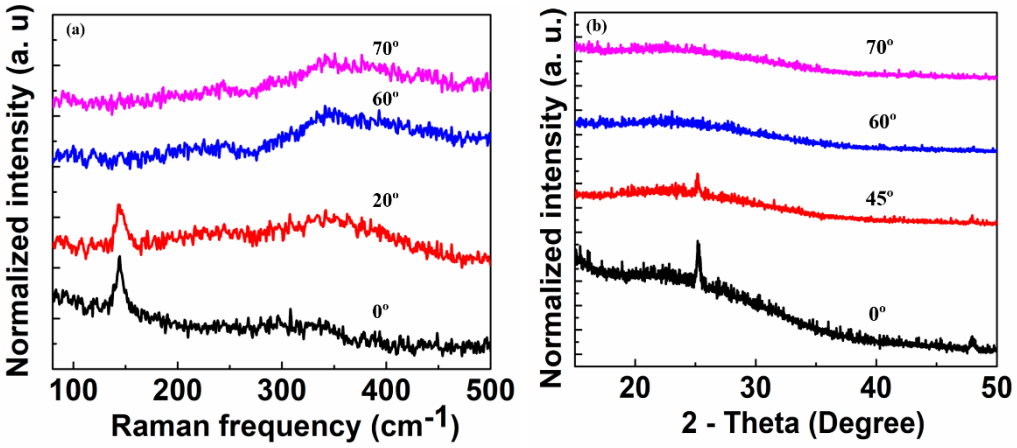

Figure 5. (a) Raman spectra and (b) XRD patterns of TiO_2 thin films with different incident angles.

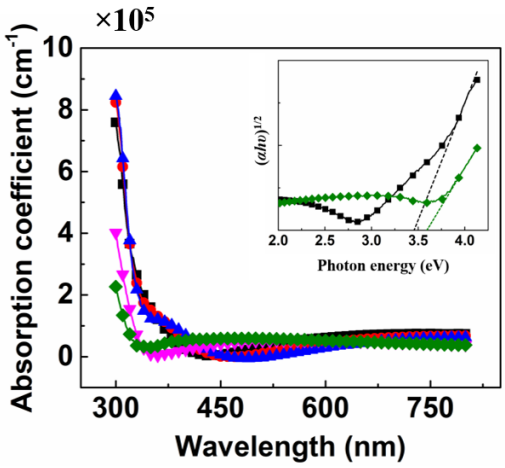

Figure 6. Absorption coefficient spectra of TiO_2 thin films with incident angles 0º (rectangles), 20º (circles), 45º (up-point triangles), 60º (down-point triangles), and 70º (rhombuses). The inset is Tauc's plot - $(\alpha hv)^{1/2}$ versus photon energy plot of TiO_2 thin films with incident angles of 0º and 70º.

Figure 6 shows absorption coefficient spectra of the TiO_2 thin films with the different incident angles. The PED-fabricated TiO_2 thin films possessed a relatively high absorption coefficient (5.5×10^5 cm^{-1}) at around 310 nm [39]. However, the absorption coefficient at 310 nm was reduced to 1.3×10^5 cm^{-1} when the incident angles increased from 0º to 70º. Furthermore, the Tauc's plot, as shown in inset on Figure 6, implied that the indirect band gap

energy of the fabricated TiO_2 thin films increased from 3.45 to 3.59 eV as the incident angles increased from 0º to 70º. While decreasing in the absorption coefficient was probably resulted from reducing in the thin film density, which is good agreement with the aforementioned Raman and SEM data, increasing in the band gap energy was probably resulted from the relatively low sizes of TiO_2 nanoparticles [40]. We suggested that as the incident angle increased, the TiO_2 nanoparticles were inclined to grow in perpendicular direction; thereby, the TiO_2 nanoparticle sizes were reduced and the band gap energies were enlarged. Figure 7 exhibits the normalized PL spectra of the PED-fabricated TiO_2 thin films with the different incident angles. By increasing the incident angles from 0º to 70º, the PL peaks were blue-shifted from 413 to 398 nm. As the band gap energies were directly proportional to the incident angles, the TiO_2 thin films deposited with the relatively high incident angles (60º or 70º) absorbed and radiated the shorter-wavelength photon.

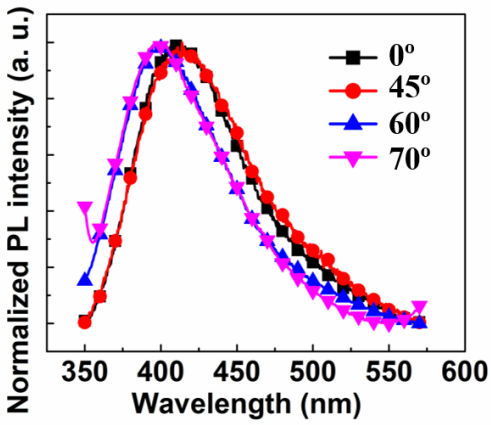

Figure 7. Normalized PL spectra of TiO_2 thin films with various incident angles.

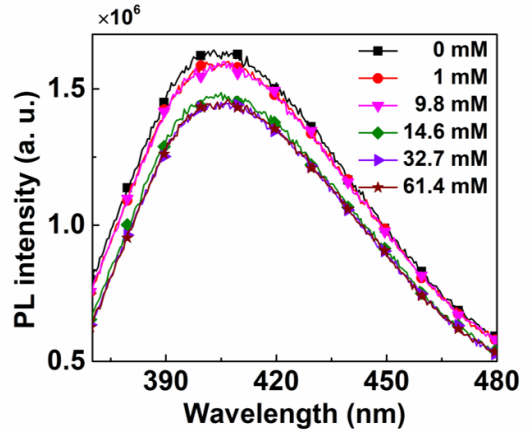

Figure 8. PL spectra of PED-based TiO_2 thin film immersed in glucose solutions with different concentrations.

In order to explore and verify the material potentials, the PED-fabricated TiO_2 thin films without GLAD techniques were used for simple non-enzymatic glucose sensing. In particular, glucose was detected through the PL quenching of the TiO_2 thin films under 315-nm wavelength light irradiation. Figure 8 shows the PL spectra of the fabricated TiO_2 thin films with the glucose

solutions. We note that the concentration of glucose solutions was altered from 1 to 61.4 mM and that there were no additional enzymes used. It indicated that the PL intensities were degraded by increasing the glucose concentrations and there was no significant change in the PL-peak position observed. Although more efforts should be required to understand the PL quenching mechanisms, we suggested that the TiO_2 thin films and ultra violet (UV) irradiation probably act as the catalysts to oxidize the glucose [39]. In this study, UV light (wavelength of 315 nm) played two important roles: (*i*) excitation for PL emission and (*ii*) UV irradiation for glucose oxidation. Under UV excitation, electrons and holes were photo-generated into the conduction band and valence band of the TiO_2 thin films, respectively. In general, those carriers intended to recombine and emit photons with wavelength of 413 nm, but they oxidized glucose into gluconic acid and H_2O_2 when the excited TiO_2 thin films were immerged into the glucose solution under UV irradiation. Those oxidation processes then prevented the radiative recombination of the photo-generated carriers and led to the aforementioned PL quenching phenomena [41].

4. CONCLUSIONS

A study on fabrication and characterization of the TiO_2 thin films using PED was reported. The fabricated TiO_2 thin films were formed in anatase phases with the crystallite sizes of around 20.3 nm and the energy band gap of 3.45 eV, which implied that the sizes of the nanoparticles in the thin films were relatively small. Furthermore, the effects of GLAD techniques on the crystallite structure, surface morphology, and the optical and electronic properties of the PED-fabricated TiO_2 thin films were demonstrated. By increasing incident angles, the rod-like nanoparticles seemed to be risen up, the absorption coefficient decreased, the energy band gap increased, and the Raman peaks at 144 cm^{-1} in TiO_2 thin films were disappeared. We suggested that those results resulted from the voiding sites appearing during the growth of obliquely deposited TiO_2 thin films. Furthermore, the non-enzymatic fluorescent biosensor for glucose sensing using the PED-based TiO_2 thin films was demonstrated to explore the application potential of the fabricated materials. The PL intensities were degraded when the excited TiO_2 thin films were immersed into the glucose solution under UV irradiation.

Acknowledgements. The authors have no relevant financial or non-financial interests to disclose.

CRediT authorship contribution statement. Quang-Duy Dao: Supervision. Tri-Nghia Nguyen: Methodology, Investigation. Duy Thien Nguyen: Methodology, Investigation. Tung Nguyen Dinh Hai: Formal analysis. Thi Huong Vu: Formal analysis. Tuan Tu Le: Formal analysis. Thanh Mai Vu: Formal analysis. Van Vu Le: Supervision.

Declaration of competing interest. The authors declare that they have no known competing financial interests or personal relationships that could have appeared to influence the work reported in this paper.

REFERENCES

1. Hashimoto K., Irie H., and Fujishima A. - TiO_2 Photocatalysis: A Historical Overview and Future Prospects, Jpn. J. Appl. Phys. **12** (2005) 8269. DOI:10.1143/JJAP.44.8269
2. Guo Q., Zhou C., Ma Z., and Yang X. - Fundamentals of TiO_2 Photocatalysis: Concepts, Mechanisms, and Challenges, Adv. Mater. **31** (2019) 1901997. DOI:10.1002/ adma.201901997

3. Dao Q. D., Fujii A., Tsuji R., and Ozaki M. - Highly efficient perovskite solar cell utilizing a solution-processable tetrabenzoporphyrin hole transport material with p-type dopants, Appl. Phys. Express **12** (2019) 112009. DOI: 10.7567/1882-0786/ab4aa2
4. Homola T., Pospisil J., Shekargoftar M., Svoboda T., Hvojnik M., Gemeiner P., Weiter M., and Dzik P. - Perovskite Solar Cells with Low-Cost TiO_2 Mesoporous Photoanodes Prepared by Rapid Low-Temperature (70 °C) Plasma Processing, ACS Appl. Energy Mater. **3** (2020) 12009. DOI:10.1021/acsaem.0c02144
5. Dao Q.-D., Tsuji R., Fujii A., and Ozaki M. - Study on degradation mechanism of perovskite solar cell and their recovering effects by introducing CH_3NH_3I layers, Org. Electron. **43** (2017) 229. DOI:10.1016/j.orgel.2017.01.038
6. El-Deen S. S., Hashem A. M., Abdel Ghany A. E., Indris S., Ehrenberg H., Mauger A., and Julie C. M. - Anatase TiO_2 nanoparticles for lithium-ion batteries, Ionics **24** (2018) 2925. DOI:10.1007/s11581-017-2425-y
7. Khatim O., Amamra M., Chhor K., Bell A.M.T., Novikov D., Vrel D., and Kanaev A. - Amorphous–anatase phase transition in single immobilized TiO_2 nanoparticles, Chem. Phys. Lett. **558** (2013) 53. DOI:10.1016/j.cplett.2012.12.019
8. Li Z., Cong S., and Xu Y. - Brookite vs Anatase TiO_2 in the Photocatalytic Activity for Organic Degradation in Water, ACS Catal. **4** (2014) 3273. DOI:10.1021/cs500785z
9. Luttrell T., Halpegamage S., Tao J., Kramer A., Sutter E., and Batzill M. - Why is anatase a better photocatalyst than rutile? - Model studies on epitaxial TiO_2 films, Sci Rep **4** (2014) 4043. DOI: 10.1038/srep04043
10. Regraguy B., Rahmani M., Mabrouki J., Drhimer F., Ellouzi I., Mahmou C., Dahchour A., Mrabet M. E., and Hajjaji S. E. - Photocatalytic degradation of methyl orange in the presence of nanoparticles $NiSO_4/TiO_2$, Nanotechnol. Environ. Eng. **7** (2022) 157. DOI:10.1007/s41204-021-00206-0.
11. Lee S. Y., Kang D., Jeong S., Do H. T., and Kim J. H. - Photocatalytic Degradation of Rhodamine B Dye by TiO_2 and Gold Nanoparticles Supported on a Floating Porous Polydimethylsiloxane Sponge under Ultraviolet and Visible Light Irradiation, ACS Omega **5** (2020) 4233. DOI:10.1021/acsomega.9b04127
12. Suligoj A., Kete M., Cernigoj U., Fresno F., and Stangar U. L. - Synergism in TiO_2 photocatalytic ozonation for the removal of dichloroacetic acid and thiacloprid, Environ. Res. **197** (2021) 110982. DOI:10.1016/j.envres.2021.110982
13. Tan S., Feng H., Ji Y., Wang Y., Zhao J., Zhao A., Wang B., Luo Y., Yang J., and Hou J. G. - Observation of Photocatalytic Dissociation of Water on Terminal Ti Sites of TiO_2(110)-1 × 1 Surface, J. Am. Chem. Soc. **134** (2012) 9978. DOI:10.1021/ja211919k
14. Grochowska K., Ryl J., Karczewski J., Śliwiński G., Cenian A., and Siuzdak K. J. - Non-enzymatic flexible glucose sensing platform based on nanostructured TiO_2/Au composite, J. Electroanalytical Chem. **837** (2019) 230. DOI:10.1016/j.jelechem.2019.02.040
15. Jeong H., Yoo J., Park S., Lu J., Park S., and Lee J. - Non-Enzymatic Glucose Biosensor Based on Highly Pure TiO_2 Nanoparticles, Biosensors **11** (2021) 149. DOI:10.3390/bios11050149
16. Dao Q. D., Fujii A., Tsuji R., and Ozaki M. - A study on solution-processable tetrabenzomonoazaporphyrin hole transport material for pervoskite solar cells, Adv. Nat. Sci.: Nanosci. Nanotechnol. **11** (2020) 015007. DOI:10.1088/2043-6254/ab6c4d

17. Xu Y., Gao C., Tang S., Zhang J., Chen Y., Zhu Y., and Hu Z. - Comprehensive understanding of $TiCl_4$ treatment on the compact TiO_2 layer in planar perovskite solar cells with efficiencies over 20%, J. of Alloys Compd. **787** (2019) 1082. DOI:10.1016/j.jallcom.2019.02.027
18. Murakami T. N., Miyadera T., Funaki T., Cojocaru L., Kazaoui S., Chikamatsu M., and Segawa H. - Adjustment of Conduction Band Edge of Compact TiO_2 Layer in Perovskite Solar Cells Through $TiCl_4$ Treatment, ACS Appl. Mater. Interfaces **9** (2017) 36708. DOI:10.1021/acsami.7b07496
19. Dao Q. D., Fujii A., Tsuji R., Takeoka Y., and Ozaki M. - Efficiency enhancement in perovskite solar cell utilizing solution-processable phthalocyanine hole transport layer with thermal annealing, Org. Electron. **43** (2017) 156. DOI:10.1016/j.orgel.2017.01.027
20. Cargnello M., Gordon T. R., and Murray C. B. - Solution-Phase Synthesis of Titanium Dioxide Nanoparticles and Nanocrystals, Chem. Rev. **114** (2014) 9319. DOI:10.1021/ cr500170p
21. Pradhan S. K., Reucroft P. J., Yang F., and Dozier A. - Growth of TiO_2 nanorods by metalorganic chemical vapor deposition, J. Cryst. Growth **256** (2003) 83. DOI:10.1016/S0022-0248(03)01339-3
22. Kumi-Barimah E., Penhale-Jones R., Salimian A., Upadhyaya H., Hasnath A., and Jose G. - Phase evolution, morphological, optical and electrical properties of femtosecond pulsed laser deposited TiO_2 thin films, Sci. Rep. **10** (2020) 10144. DOI:10.1038/s41598-020-67367-x
23. Lee S. W., Bae S., Cho K., Kim S., Hwang J. K., Lee W., Lee S., Hyun J. Y., Lee S., Choi S. B., Chun H., Kim W. M., Kang Y., Lee H. S., and Kim D. - Sputtering of TiO_2 for High-Efficiency Perovskite and 23.1% Perovskite/Silicon 4-Terminal Tandem Solar Cells, ACS Appl. Energy Mater. **2** (2019) 6263. DOI:10.1021/acsaem.9b00801
24. Sanz M., Walczak M., Oujja M., Cuesta A., and Castillejo M. - Nanosecond pulsed laser deposition of TiO_2: nanostructure and morphology of deposits and plasma diagnosis, Thin Solid Films **517** (2009) 6546. DOI:10.1016/j.tsf.2009.04.026
25. Walczak M., Papadopoulou E. L., Sanz M., Manousaki A., Marco J. F., and Castillejo M. - Structural and morphological characterization of TiO_2 nanostructured films grown by nanosecond pulsed laser deposition, Appl. Surf. Sci. **255** (2009) 5267. DOI:10.1016/j.apsusc.2008.07.098
26. Walczak M., Oujja M., Marco J. F., Sanz M., and Castillejo M. - Pulsed laser deposition of TiO_2: diagnostic of the plume and characterization of nanostructured deposits, Appl Phys A **93** (2008) 735. DOI:10.1007/s00339-008-4704-y
27. Xie Z., Zhao F., Zou S., Zhu F., Wang W., and Zhang Z. - TiO_2 nanorod arrays decorated with Au nanoparticles as sensitive and recyclable SERS substrates, J. Alloys Compd. **861** (2021) 157999. DOI:10.1016/j.jallcom.2020.157999
28. Zhou Q., He Y., Abell J., Zhang Z., and Zhao Y. - Surface-enhanced Raman scattering from helical silver nanorod arrays Chem. Commun. **47** (2011) 4466. DOI:10.1039/ C0CC05465H
29. Vick D., Friedrich L. J., Dew S. K., Brett M. J., Robbie K., Seto M., and Smy T. - Self-shadowing and surface diffusion effects in obliquely deposited thin films, Thin Solid Films **339** (1999) 88. DOI:10.1016/S0040-6090(98)01154-7

30. Praveen P., Viruthagiri G., Mugundan S., and Shanmugam N. - Structural, optical and morphological analyses of pristine titanium di-oxide nanoparticles – Synthesized via sol–gel route, Spectrochim. Acta A **117** (2014) 622. DOI:10.1016/j.saa.2013.09.037
31. Dao Q. D., Fujii A., Tsuji R., Pham N. H., Bui H. V., Sai C. D., Nguyen D. T., Vu T. H., and Ozaki M. - Mesoporous TiO_2 electron transport layer engineering for efficient inorganic-organic hybrid perovskite solar cells using hydrochloric acid treatment, Thin Solid Films **732** (2021) 138768. DOI:10.1016/j.tsf.2021.138768
32. Ranga Rao A., and Dutta V. - Low-temperature synthesis of TiO_2 nanoparticles and preparation of TiO_2 thin films by spray deposition, Sol. Energy Mater Sol. Cells **91** (2007) 1075. DOI:10.1016/j.solmat.2007.03.001
33. Kathiravan A., and Renganathan R. - Photosensitization of colloidal TiO_2 nanoparticles with phycocyanin pigment, J. Colloid Interface Sci **335** (2009) 196. DOI:10.1016/j.jcis.2009.03.076
34. Shown I., Ujihara M., and Imae T. - Sensitizing of pyrene fluorescence by β-cyclodextrin-modified TiO_2 nanoparticles, J. Colloid Interface Sci **352** (2010) 232. DOI:10.1016/j.jcis.2010.08.055
35. Parayil S. K., Kibombo H. S., Wu C. M., Peng R., Baltrusaitis J., and Koodali R. T. - Enhanced photocatalytic water splitting activity of carbon-modified TiO_2 composite materials synthesized by a green synthetic approach, Int. J. Hydrogen Energy **37** (2012) 8257. DOI:10.1016/j.ijhydene.2012.02.067
36. Pooja P., and Chinnamuthu P. - Annealing Effect of Glancing Angle Electron Beam Deposited TiO_2/In_2O_3 Nanowires Array on Surface Wettability, Sci. Rep. **10** (2020) 9416. DOI: 10.1038/s41598-020-66150-2
37. Sanchez-Valencia J. R., Longtin R., Rossell M. D., and Groening P. - Growth assisted by glancing angle deposition: a new technique to fabricate highly porous anisotropic thin films, ACS Appl. Mater. Interfaces **8** (2016) 8686. DOI:10.1021/acsami.6b00232
38. Lagopati N., Tsilibary E. P., Falaras P., Papazafiri P., Pavlatou E. A., Kotsopoulou E., and Kitsiou P. - Effect of nanostructured TiO_2 crystal phase on photoinduced apoptosis of breast cancer epithelial cells, Int J Nanomedicine **9** (2014) 3219. DOI:10.2147/IJN.S62972
39. Cui L., Wang W. - Optical properties of anatase and rutile TiO_2 films deposited by using a pulsed laser, Appl. Opt. **60** (2021) 8453. DOI:10.1364/AO.437646
40. Pyun M. W., Kim E. J., Yoo D. H., and Hahn S. H. - Oblique angle deposition of TiO_2 thin films prepared by electron-beam evaporation, Appl. Surf. Sci. **257** (2010) 1149. DOI:10.1016/j.apsusc.2010.08.038
41. Sodzel D., Khranovskyy V., Beni V., Turner A. P. F., Viter R., Eriksson M. O., Holtz P.-O., Janot J. M., Bechelany M., Balme S., Smyntyna V., Kolesneva E., Dubovskaya L., Volotovski I., Ubelis A., and Yakimova R. - Continuous sensing of hydrogen peroxide and glucose via quenching of the UV and visible luminescence of ZnO nanoparticles, Microchim Acta **182** (2015) 1819. DOI:10.1007/s00604-015-1493-9